Journal of Wind Engineering
and Industrial Aerodynamics 96 (2008) 1–24

JOURNAL OF wind engineering AND industrial aerodynamics

www.elsevier.com/locate/jweia

The methodology for aerodynamic study on a small domestic wind turbine with scoop

F. Wang[a,*], L. Bai[a], J. Fletcher[b], J. Whiteford[c], D. Cullen[c]

[a]*School of the Built Environment, Heriot-Watt University, Edinburgh, EH14 4AS, UK*
[b]*School of Engineering and Physics Sciences, Heriot-Watt University, Edinburgh, UK*
[c]*Dynamic Wind Generators Ltd, Fife, UK*

Received 11 April 2006; received in revised form 12 February 2007; accepted 14 March 2007
Available online 4 May 2007

Abstract

The aim of this study is to investigate the possibility of improving wind energy capture, under low wind speed conditions, in a built-up area, and the design of a small wind generator for domestic use in such areas. This paper reports the first part of this study: the development of the methodology using physical tests conducted in a boundary layer wind tunnel and computer modelling using commercial computational fluid dynamics (CFD) code. The activities reported in this paper are optimisation of a scoop design and validation of the CFD model. The final design of scoop boosts the airflow speed by a factor of 1.5 times equivalent to an increase in power output of 2.2 times with the same swept area. Wind tunnel tests show that the scoop increases the output power of the wind turbine. The results also indicate that, by using a scoop, energy capture can be improved at lower wind speeds. The experimentally determined power curves of the wind generator located in the scoop are in good agreement with those predicted by the CFD model. This suggests that first the developed computer model was robust and could be used later for design purposes. Second the methodology developed here could be validated in a future study for a new rotor blade system to function well within the scoop. The power generation of such a new wind turbine is expected to be increased, particularly at locations where average wind speed is lower and more turbulent. The further study will be reported elsewhere.

Keywords: Scoop; Diffuser; Wind tunnel test; Small domestic wind turbine; Computational fluid dynamics (CFD)

*Corresponding author. Tel.: +44 1314494636; fax: +44 1314513161.
E-mail address: fan.wang@hw.ac.uk (F. Wang).

0167-6105/$ - see front matter
doi:10.1016/j.jweia.2007.03.004

Nomenclature

A	swept area (m^2)
C_p	power coefficient, $C_p = P_s/(\frac{1}{2}\rho A U_0^3)$
F	electrical frequency (Hz)
$\vec{F}_p, \vec{F}_v$	pressure and viscous force vector (N)
M	moment acting on the blades (Nm)
P	static pressure (Pa)
P_s	shaft power output (W)
R	tip radius of rotor (m)
U_0	upstream undisturbed wind speed ($m\,s^{-1}$)
U_e	wind speed at entrance of the scoop ($m\,s^{-1}$)
U_c	wind speed at cylinder part of the scoop ($m\,s^{-1}$)
P	density of the air ($kg\,m^{-2}$)
Λ	tip speed ratio $\lambda = \Omega R/U$
Ω	angular velocity ($rad\,s^{-1}$)

1. Introduction

The increasing awareness of the general public to climate change and global warming has provided opportunities for wind turbine applications in the UK. The UK claims 40% of the wind energy resources of Europe. Europe leads the world with 70.3% (23 GW peak) of the total operational wind power capacity worldwide (Ackermann and Soder, 2002). As well as large wind turbines operating in open areas on- and off-shore, more small-scale wind turbines are being installed and operated by homeowners and small enterprises. Small-scale wind turbines generating electricity have seen sales grow an average of 40% per year since the energy crisis of the 1970s (AWEA, 2002). The UK has several small wind turbine manufacturers with rotor diameters ranging from 0.5 to 11 m (European Commission, 2004).

One of the differences between large- and small-scale wind turbines is that small-scale wind turbines are generally located where the power is required, often within a built environment, rather than where the wind is most favourable. In such location, the wind is normally weak, turbulent and unstable in terms of direction and speed, because of the presence of buildings and other adjacent obstructions. To yield a reasonable power output from a small-scale wind turbine located in this turbulent environment, and to justify such an installation economically, the turbines have to improve their energy capture, particularly at low wind speeds and be responsive to changes in wind direction. This means that small-scale turbines need to be specifically designed to work effectively in low and turbulent wind resource areas. Currently, manufacturers of small wind turbines in the UK are not seen to make an attempt to accelerate low-speed airflow prior to reaching the turbines rotating blades.

As power output is proportional to the cubic power of the incident airspeed, any small increase in the incident wind yields a large increase in the energy output. Consequently, many research groups have attempted to exploit this relationship. Such studies include adding a diffuser to the wind turbine from the early 1980s (Gilbert and Foreman, 1983) to the beginning of this century (Phillips et al., 2000) (Hansen et al., 2000). More recently, Ohya et al. (2002, 2004) have produced an effective wind-acceleration system. The system contains a large diffuser with a flange creating a large separation in the flow. This generates a low-pressure region which assists the turbine in capturing more wind energy compared to a system with a diffuser on its own. From experimental research conducted on this system it is shown that a diffuser–shrouded wind turbine generates more power compared to a bare wind turbine, with a power coefficient four times higher (Abe et al., 2005). It is also shown that the downstream of the wind turbine the typical vortex structure created by a bare wind turbine is easily dispersed by the use of the diffuser, which is another feature that assists wind energy capture of the wind turbine. Other research groups have found that the wind speed in a diffuser is significantly influenced by the length and expansion angle of the diffuser and with an optimum design can create a wind speed improvement of 1.7 times (Matsushima et al., 2006).

In addition to the difficulty of working in weak and turbulent airflows, another problem which faces small-scale wind turbines is to start the rotor system at low airspeeds. Wind turbines with the small blade radius have a very small aerodynamic starting torque, which often has to overcome significant brush friction torque with DC generators or cogging torques associated with permanent magnet (PM) generators. Starting can be improved by accelerating the airspeed through the blade system. Some work has been published on wind turbine starting (Wright and Wood, 2004; Mayer et al., 2001; Wood, 2001; Ebert and Wood, 1997; Clausen and Wood, 2000). Wright and Wood (2004) have measured the starting performance of a three bladed, 2 m diameter horizontal axis wind turbine in field tests. Generic equations for lift and drag coefficients have been employed to predict rotor acceleration and deceleration and excellent agreement is found between the theory and tests. Their findings suggest that small wind turbines normally start rotating at about 4.6 m/s. Unfortunately this value is higher than the average wind speed in most built environments.

Parallel to design of the small-scale wind turbines, assessment of their performance is also critical. Currently there is a lack of standard methods of assessment. The standard methods of assessment are developed for large wind turbines, which are typically operated in open areas where the wind is stronger and more stable than that in the built environment. It is rather problematic to apply such methods to small wind turbines working in built environment flows. As a result, the estimated annual output for small wind turbines varies from modest figures, like 1300 kW h (PROVEN, 2.5 m rotor diameter) (PROVEN, 2006) to figures like 4000 kW h (SWIFT, 2.1 m rotor diameter) (SWIFT, 2006). There is a need to formalize a standard method of performance assessment that is reasonable for small wind turbines working in built environments.

Although small-scale wind turbines are assessed using three aspects: safety and functions, durability (IEC, 1996) and power performance (IEC, 1997), the latter plays a more active role in guiding its aerodynamic design. The power performance of a wind turbine can normally be measured in two ways: monitor it on a real site or test it in a wind tunnel. Field monitoring gives more realistic results, but needs complicated and robust instrumentation, takes a longer period to cover various wind conditions, and a systematical analysis on large data sets accumulated during the months of tests. Consequently this method is always more expensive than wind tunnel tests. Wind tunnel tests also have drawbacks, among which is the limitation on the size of the wind turbine being tested inside a tunnel. In order to minimise the effects of obstruction of airflow inside the tunnel, the object being tested needs to be small enough so that its blockage to the flow is negligible. Therefore, wind turbines need scaled down to fit in a specific wind tunnel. As wind tunnel test do offer many advantages, including controllable incoming wind, simpler instrumentation, and shorter test periods, the experimental phase of this project is conducted in a wind tunnel. A virtual wind tunnel using computational fluid dynamics (CFD) was also developed to tackle the blockage problem in this study.

The IEC Standard on power performance assessment (IEC, 1997) provides a good basis for accurate and consistent analysis of the performance of a wind turbine or wind farm. However, new techniques are being devised to improve the accuracy of power performance assessment. One such example is presented in a recent paper published by Riso (2001). Some of these new techniques were applied into this project where appropriate. Frandsen et al. (2000) also suggests new technique that can significantly improve the accuracy of power performance assessment. This was not used in this study as it was considered impossible to follow the methods. Imamura et al. (1999) have also completed interesting research into the problems of performance analysis on complex terrain. Beattie (2001) has discussed that the impacts of several important determinant factors including turbulence intensity, seasonal variation, wind direction and wind directional variation on wind turbine power curves by following the guidelines of IEC (1997) on power performance assessment, and power curves were produced that enabled prediction of the annual energy production (AEP) of each wind turbine and the wind farm as a whole.

Fabiano et al. (2003) carried out an investigation of laboratory and field test on AIR 430 and W20 turbines. Their results show that the power curve of the wind turbine studied is lower than the one supplied by the manufacturer, but closer to the ones found in the bibliographical references. This suggested a promising way of reducing test costs for this study. Corbus et al. (1999) described testing procedures for obtaining type certification for a small wind turbine, the AIR 403, which was the first small turbine to be certified in the United States. National Renewable Energy Laboratory (NREL) has reported the results of a power performance test on a Bergey Excel-s/60 with a Gridtek-10 Inverter and SH 3052 airfoil blades. The Bergey Excel is a three-bladed upwind turbine rated at 10 kW output at $13.0\,\mathrm{m\,s^{-1}}$. The rotor diameter is 6.17 m. The results show the highest C_p is 0.21 with incident wind speeds of 7.98 and $8.5\,\mathrm{m\,s^{-1}}$.

When applying computers to wind turbine studies, two types of computational technology have been seen. The common one is Blade Element Momentum (BEM) theory, which is a simple theoretical method developed for blade optimisation and rotor design. The other is CFD, where Navier–Stokes equations are solved together with some turbulence models approximating wind turbulence to reveal the global flows. The results of such modelling are impressive with large amounts of data detailing the flow domain. The difficulty of using such a method is computing costs, particularly when good resolution is needed near the blades. Therefore for design, when the flows near the blades are of concern, some simple theoretical methods are proposed to simplify this procedure. Using CFD, Abea et al. (2004) carried out numerical investigations of flow fields behind a small wind turbine with a flanged diffuser. Their representation of the rotor uses a disk loading method, which is also used in other studies (Sorensen and Kock, 2004; Kume et al., 2003). Mandas et al. (2005) have modelled a real three-dimensional large-scale wind turbine using Fluent, and compared the results with those obtained from the BEM theory. These are in good agreement.

In this study, due to the involvement of the scoop which alters airflow, CFD appeared more appropriate as a modelling tool. Therefore, this study applied both experimental and numerical methods to develop a new methodology to test small-scale wind turbines. The power performance is the key variable examined closely in both the wind tunnel tests and CFD modelling. The procedure is described in Section 2 which includes scoop design and development of the CFD model. Results and discussion are provided in Section 3, and conclusions in Section 4.

2. Methodology

Fig. 1 shows the flow chart and gives an overall view of the methodology used in this investigation. All activities and their objectives are as follows.

Activities 1 and 2 are related to scoop design. The scoop accelerates the airspeed in a residential area hence provides more energy in the lower part of the boundary layer, where wind is weak and turbulent in a built-up area. The objective of this activity is to find a suitable scoop, characterised by its shape and profile, to boost wind speed. This was facilitated using CFD modelling. The final design obtained from the CFD modelling was manufactured and tested in the Wind Tunnel at Heriot-Watt University. The test results are used to validate the CFD modelling. In the wind tunnel test, the pressure and velocity distribution are measured and compared against the CFD predicted results. Good agreement confirms the robustness of the CFD technique.

Activities 3 and 4 are to develop a CFD method to be used as a virtual wind tunnel to test various design options of wind turbine and their effects on power output of the turbine. A small wind turbine (Rutland 913 windcharger) from a previous study was used to reduce the cost. It has swept area of 0.65 m^2 (0.91 in diameter), among which 0.045 m^2 (7%) is taken by its nacelle. It is rated to produce 24 W at wind speed of 10 knots (5.15 m/s) and

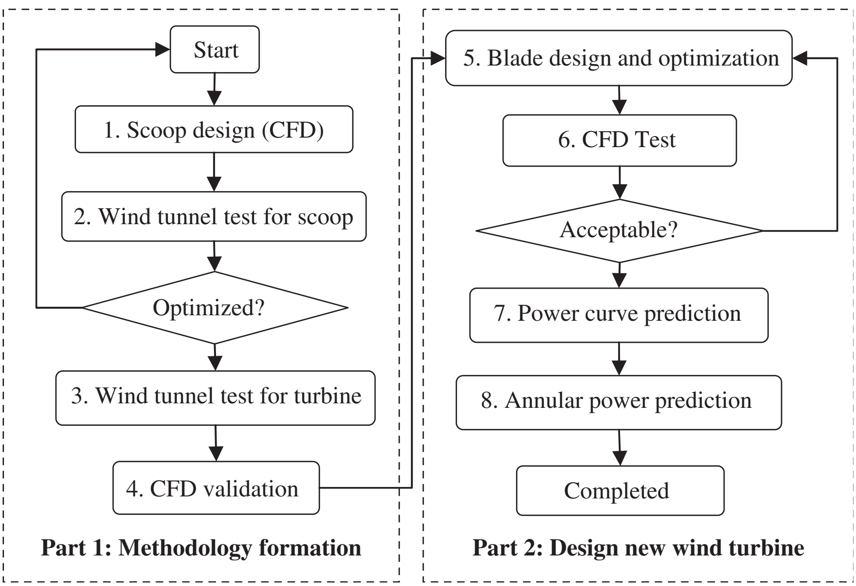

Fig. 1. Flow chart of design methodology.

90 W at 19 knots (9.8 m/s). Its blades were later trimmed to fit into the scoop and tested in the wind tunnel. The pressure distribution and power curves were measured to validate the CFD models developed. The CFD model involved: defining domain and boundary conditions, creating boundary layers for blade surfaces and rotating mesh system, and processing data to calculate torque of the rotor, hence power output.

Activities 5 and 6 find the optimised design of the rotor, consisting of the blade, nose cone and nacelle. The blade shape was designed using BEM theory. The power performance was predicted by a CFD model developed using the method established in Part 1 of this study.

Activities 7 and 8 predict the annual power output of the finalised design using statistical wind data (in this case for Edinburgh), where hourly wind speed was counted to calculate the cumulated power production of the turbine.

2.1. Scoop design

The objective of the scoop design is to use CFD to find a scoop profile that achieves the highest acceleration, hence gain in airflow energy. The model was also tested in wind tunnel, so that the CFD prediction and wind tunnel measurements could be compared to validate the computer model.

2.1.1. Modelling cases for scoop parametric study

The specifications of the designs studied are shown in Table 1 and features, including the profiles and dimensions, are illustrated in Fig. 2.

2.2. The computational model for the scoop

The CFD model included the scoop and the domain (Fig. 3) and was developed using Fluent. Due to circumferential symmetry, only a quarter of the scoop and associated area are modelled. The computational domain did not take the dimension of the wind tunnel, as it was considered slightly too small to accommodate the existing turbine and the scoop. Therefore, the modelled domain was made cylindrical and had a radius of 8.3 times that of the scoop and a diameter five times the scoop, in order to minimise the blockage problem.

Table 1
Key geometric parameters of nine scoops tested

No	Entrance (mm)	Cylinder (mm)	Exit (mm)
1	$\Phi = 6000$, $L = 1000$	$\Phi = 4000$	$\Phi = 5000$, $L = 1000$
2	$\Phi = 6000$, $L = 2000$	$\Phi = 4000$, $L = 2000$	$\Phi = 5000$, $L = 500$
3	$\Phi = 6000$, $L = 2500$	$\Phi = 4000$, $L = 2500$	$\Phi = 5000$, $L = 1000$
4	$\Phi = 6000$, $L = 2000$	$\Phi = 4000$, $L = 2000$	$\Phi = 6000$, $L = 2000$
5	$\Phi = 6000$, $L = 2000$	$\Phi = 2000$, $L = 2000$	$\Phi = 6000$, $L = 2000$
6	$\Phi = 6000$, $L = 2000$ with specified profile	$\Phi = 4000$, $L = 2000$	$\Phi = 6000$, $L = 2000$ with specified profile
7	$\Phi = 6000$, $L = 2000$ with specified profile	$\Phi = 4000$, $L = 1000$	$\Phi = 6000$, $L = 1500$ with specified profile
8	$\Phi = 6000$, $L = 2000$ with specified profile	$\Phi = 4000$, $L = 1500$	$\Phi = 6000$, $L = 1500$ with specified profile
9	$\Phi = 6000$, $L = 2000$ with profile in excel file	$\Phi = 4000$, $L = 1000$	$\Phi = 6000$, $L = 2000$ with specified profile

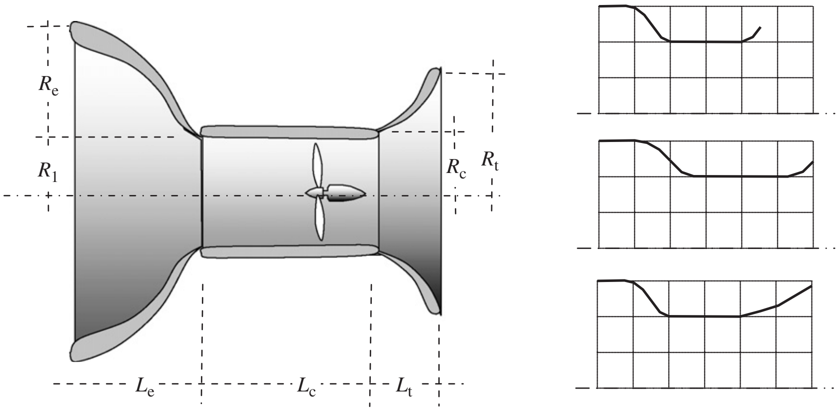

Fig. 2. Profiles and dimensions of the scoop.

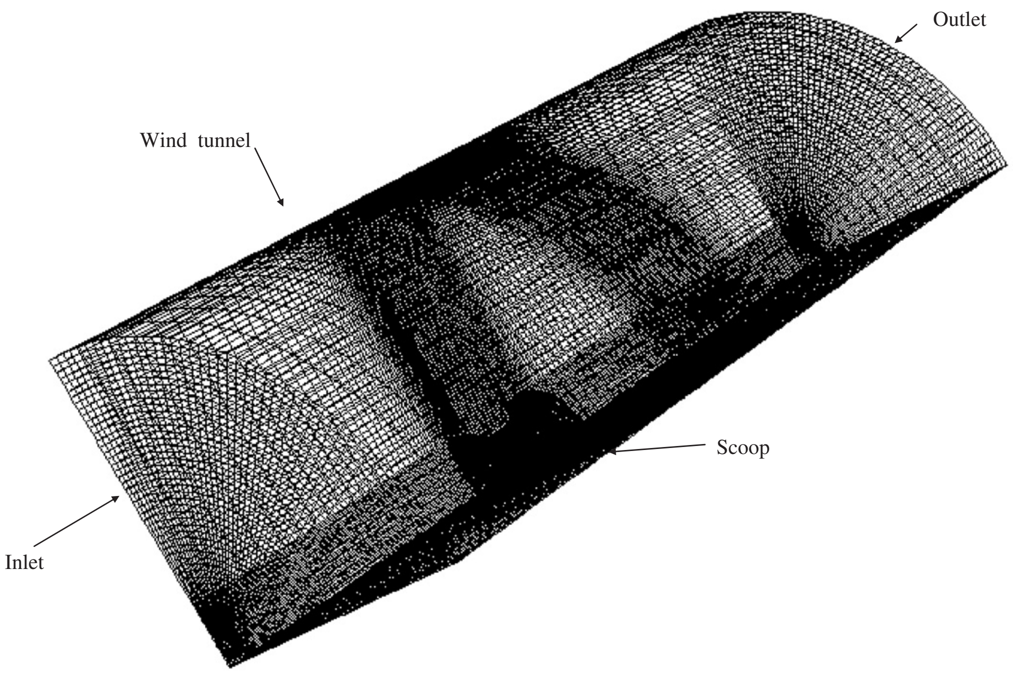

Fig. 3. The domain, grid system and boundary conditions of the CFD model for optimising the profile of the scoop.

The front and the end boundaries of the domain were defined as velocity inlet and pressure outlet, respectively, and the two circumferential surfaces as the periodical boundary conditions. The rotor of the wind turbine inside the scoop was simplified as a porous sheet with a face permeability of 1×10^{10} and pressure jump coefficient of 100 (Abe et al., 2004; Sorensen and Kock, 2004; Kume et al., 2003).

Hextetrahedral elements were used to mesh the domain, resulting in a 38,400 cell mesh (Fig. 3). RNG k–ε turbulence model was selected for all simulations.

2.2.1. Model validation with wind tunnel tests

The finalised scoop in the parametric study was fabricated: length, 0.915 m; diameter of entrance, 0.917 m and diameter of middle section, 0.613 m. It was tested in the wind tunnel with a test section of $1.5\,\mathrm{m} \times 3.25\,\mathrm{m} \times 10\,\mathrm{m}$. The tests provided measured data to compare against the CFD model. The variables measured are the pressure distribution along the inner wall of the scoop and the velocity along the centreline parallel to the wind, and along the outlet diameter perpendicular to the flow, respectively, under three incident wind speeds 9.1, 11.25 and $13.9\,\mathrm{m\,s^{-1}}$.

The internal pressure distribution was measured over two rows of 40 points by two multiple manometers. A pitot tube was used upstream of the test piece to measure the reference wind speed and hot-wire anemometry mounted onto a traversing system was used to measure the wind speed along the centreline and across the diameter line at the scoop outlet. The hot-wire anemometer was calibrated before each measurement to account for the small variations in air temperature.

2.3. Development of the CFD method

As mentioned above, CFD was used again in the following modelling exercises where the moving blades were explicitly modelled and the pressure over the blades surfaces was used to calculate the driving force turning the rotor rotating. The objective of the development of the CFD method was to create a virtual wind tunnel in which the power output of a wind turbine could be investigated with changing design parameters (including turbines whose size was too large to be tested inside the wind tunnel). The method developed here is also expected to be used in future studies where no suitable wind tunnel facilities are readily available.

2.3.1. Wind turbine

To evaluate the ability of the scoop to convert wind energy, and also to provide a reliable base for validating the methodology, a series of wind tunnel tests were conducted to predict the power curves of a wind turbine. The small wind turbine, Rutland 913, with blades trimmed down from a diameter of 0.91–0.57 m was located inside the scoop. The new configuration was tested in the wind tunnel and modelled by the CFD method. Validation is by comparison of the shaft output power.

The curve of the power coefficient against the tip speed ratio is the most important technical characteristic of a wind turbine, as it reflects the efficiency of a turbine in converting the wind energy into electrical energy.

The power coefficient C_p is defined as

$$C_\mathrm{p} = \frac{P_\mathrm{s}}{1/2\rho\pi R^2 U_0^3} \tag{1}$$

and is the ratio between the shaft power output and the power in the incident airflow. The tip speed ratio λ is defined as

$$\lambda = \frac{\Omega R}{U_0} \quad \text{and} \quad \Omega = \frac{\pi f}{2}. \tag{2}$$

2.3.2. *Wind tunnel tests*

To obtain the power curves for the wind turbine, the data acquisition system was set up (Fig. 4). The free stream velocity was measured by the pitot tube set 2 m upstream of the wind turbine. A Voltech PM3000 ACE power analyser was used to measure the power output from the three-phase, sinusoidal PM generator in the turbine. The power analyser was connected in a three-phase, four-wire configuration. The power analyser provided a digital indication of the power dissipation in the resistive load bank which was connected in a star configuration across the output of the generator. Peak output power, for a given incident wind speed, was determined by adjusting the load resistance in order to find the maximum power point. The load bank output power was then recorded. The shaft power was then estimated by compensating for ohmic power loss in the phase resistance. Generator core losses were assumed negligible compared to ohmic losses at peak output power. The scoop (indicated by the dashed lines in Fig. 4) represents the scoop used in the test. A steel stand secured the Rutland 913 rotor to the wind tunnel floor.

To validate the pressure distribution for the CFD computations, pressures from two rows of 40 holes were obtained by connecting the tubes to a multiple manometers (Fig. 4). Tests were carried out with wind speeds of 9.1 and 11.25 m s^{-1}.

2.3.3. *The CFD model*

The virtual wind tunnel was constructed by developing the CFD method mentioned in the methodology, in which the computation was validated against the wind tunnel tests with scoop and trimmed rotor tests. The computer model was the same as the real model. A new rotor, with various design options, will be tested in the future in the virtual wind tunnel. This work is the second part of the study and will be presented elsewhere.

The computational domain shown in Fig. 5 was created in GAMBIT and Fluent. Due to the symmetry of the domain, only half of the test domain was built and modelled,

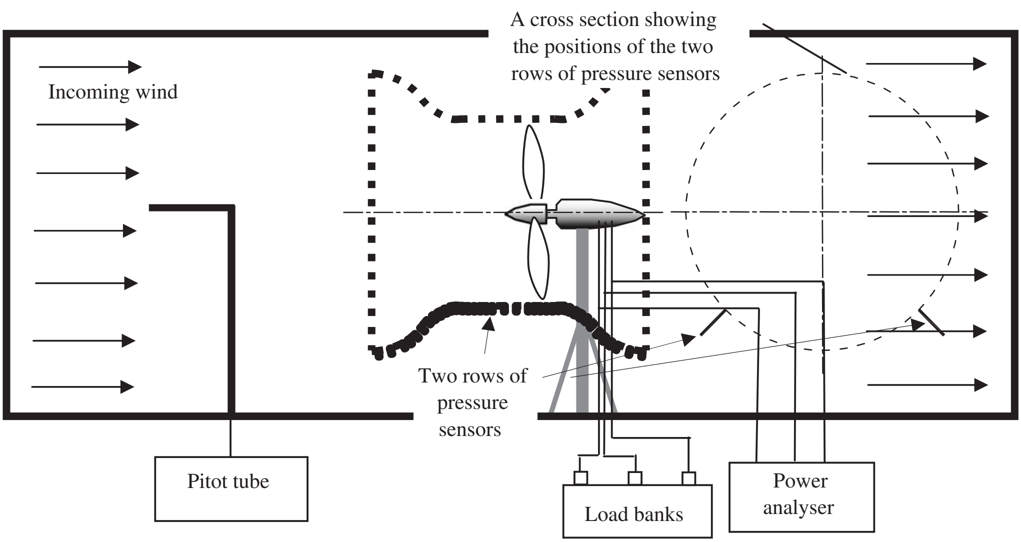

Fig. 4. Schematic diagram of the set up in the wind tunnel for the performance test.

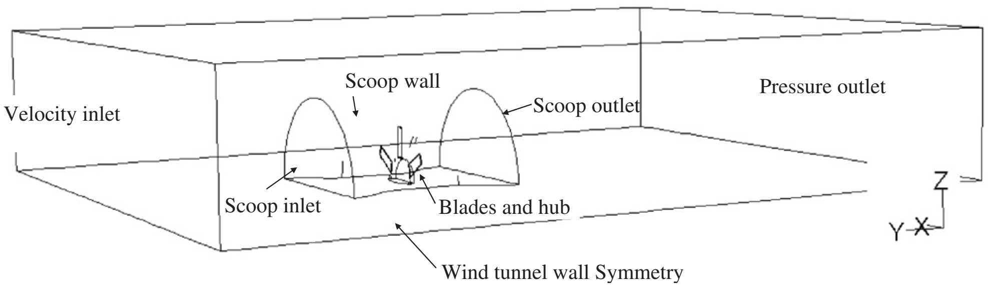

Fig. 5. Computational domain with boundary condition of the set for performance test.

extending in the axial direction 4.5 diameters of the rotor. In the direction of cross section, the domain diameter was 3.6 times that of the rotor.

Boundary conditions were set as velocity inlet and pressure outlet as shown in Fig. 5, and the symmetric boundary conditions were applied to the symmetrical plane of the domain. A uniform wind speed profile was specified at the entrance of the domain. The blades and hub were set as the rotational objects. A single reference frames (SRF) model was used to simulate the incompressible, steady-state flow field. The RNG k–ε turbulence model with standard wall functions was selected for turbulence closure.

One of the greatest challenges in this CFD modelling was to mesh the flow domain near the blades. The grids should be fine enough to capture details of geometry and flows within these critical spaces but without demanding excessive computing resources. The method applied achieved a good balance between these two aspects: fine grids were used at blade surfaces, where accurate resolution on pressure calculation was required, and also at surfaces of the scoop, and coarse grids for the rest of the domain (Fig. 6). More specifically, three boundary layers of grids were added to the blade and scoop surfaces, to simulate the turbulent flow near the walls and more accurately predict the pressure and viscous forces. The remaining spaces were discretised by tetrahedral grid elements. The total number of elements was 115,000.

2.3.4. Computation of power

Comparison between the computed and measured results for the power outputs was regarded as the ultimate validation for the CFD model developed here and could be used later as a virtual wind tunnel for other investigations of wind turbine development. The power generated by the wind turbine in the CFD model was computed during post-processing by multiplying the developed torque by the rotational speed:

$$P_{\mathrm{s}} = \vec{M}\,\Omega, \tag{3}$$

where $\vec{M}$ is the moment vector, which is computed by the following equation:

$$\vec{M} = \vec{r_{\mathrm{c}}} \times \vec{F}_{\mathrm{p}} + \vec{r_{\mathrm{c}}} \times \vec{F}_{\mathrm{v}}, \tag{4}$$

where $\vec{r_{\mathrm{c}}}$ is the vector from the centre of the hub. $\vec{F}_{\mathrm{p}}$ and $\vec{F}_{\mathrm{v}}$ are the pressure force vector and viscous force vector, respectively, which were obtained from the CFD results.

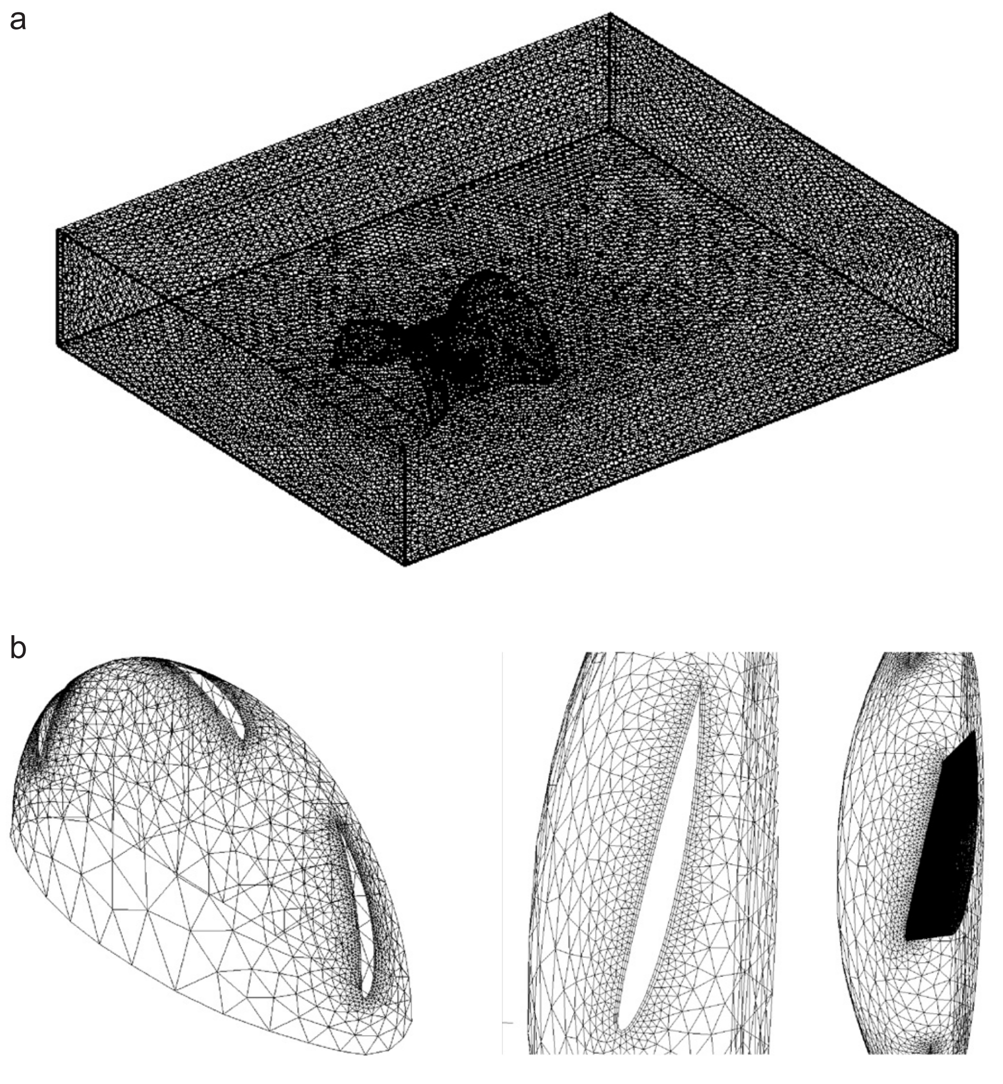

Fig. 6. The details of the mesh system created in the CFD model. (a) The mesh and geometry of the whole computational domain and (b) mesh details around the hub and the blades, in particular the boundary layers surrounding the foil surfaces.

3. Results and discussion

3.1. Scoop design and CFD validation

Scoop 6, Table 1, was the optimum among the shapes tested. It consisted of a contractor at the front, a cylinder in the middle and a diffuser at the back. The free stream velocity was accelerated by a factor of 1.5 times in the scoop according to the computational results. Such a rise in speed consequently increases the available wind energy at the wind turbine by a factor of 2.25 compared to the free stream energy with the reference speed.

The results from the CFD model were compared with the measured ones, specifically the pressure distribution along the inner surface of the scoop. Fig. 7 shows the pressure distributions at wind speeds of 11.25 and $13.9\,\mathrm{m\,s^{-1}}$, respectively. Before comparing the measured with the computed, it would be good to check the quality of the measured results. The measurement was taken in two rows which were expected to provide a better mapping over the inner surfaces of the scoop. The distributions of pressure over the two rows were consistent and in good agreement. There were small discrepancies which could be caused primarily by the slightly unsymmetrical flow over the cross sections of the scoop. This was likely as the symmetric axis of the scoop was not in good alignment with that of the wind tunnel. The evidence of this can be found by the fact that the pressures of Row A were constantly higher than those of Row B in the windward front, then constantly lower at the leeward. But in general these differences were considered acceptable hence the quality of measurement was acceptable.

When the measured data are compared with the CFD prediction, some interesting results are observed. Firstly, the main patterns of the pressure distributions obtained from the methods are in good agreement. Particularly the lowest pressure was found at exactly the same depth (0.3 m) into the scoop. The pressure rise at the contractor was also predicted well (at 0.3–04 m). The pressure dropped again when the flow was leaving the contractor and into the diffuser. The biggest differences were at the entrance and then at the diffuser. The computed results are consistently lower than the measured results. A possible reason for this could be the fact that longer tubes were used for this section of the scoop, which gave additional pressure drop, which eventually resulted in lower readings. Some discrepancies remain to be explained. Firstly, the pressure rises deeper into the scoop in the computed results (after 0.7 m) than in the measured result (before 0.7 m). Secondly, the computed results of pressure are over-estimated at the contractor, from the entrance to 0.2 m inside the scoop. Further detailed investigations may resolve these discrepancies particularly by increasing the grid density in some of the critical areas.

Velocity comparison is encouraging. Fig. 8(a) shows the velocity distributions along centreline and Fig. 8(b) across outlet of scoop at an incident speed of $11.25\,\mathrm{m\,s^{-1}}$. The distribution of air velocity along the scoop centreline was measured from the inlet to the outlet in steps of 0.04 m. The plot shows a gradual increase in airspeed until a peak is reached at a depth 0.45 m into the scoop. After passing this peak the speed reduces. The position where the highest air speed is obtained at 0.45 m is the optimum position to place a rotor. At this position the scoop could increase the free stream velocity by a factor of 1.5. The velocities measured in the tests do differ from the computed ones either being higher or lower in value. More importantly, the position where the velocity peaks still occur at the same place, approximately 0.45 m.

The velocity was also measured across the centre of the scoop outlet perpendicular to the airflow. This provides additional information on its velocity distribution (Fig. 8b). It is found that towards the edges at the outlet of the scoop the velocity was very small, virtually zero at some points, and relatively stable everywhere else. The measured data shows a rapid change in speed approaching the edges of the scoop, where such changes were much gentler in CFD prediction. Overall the magnitudes were in good agreement and the two sets results show good similarity.

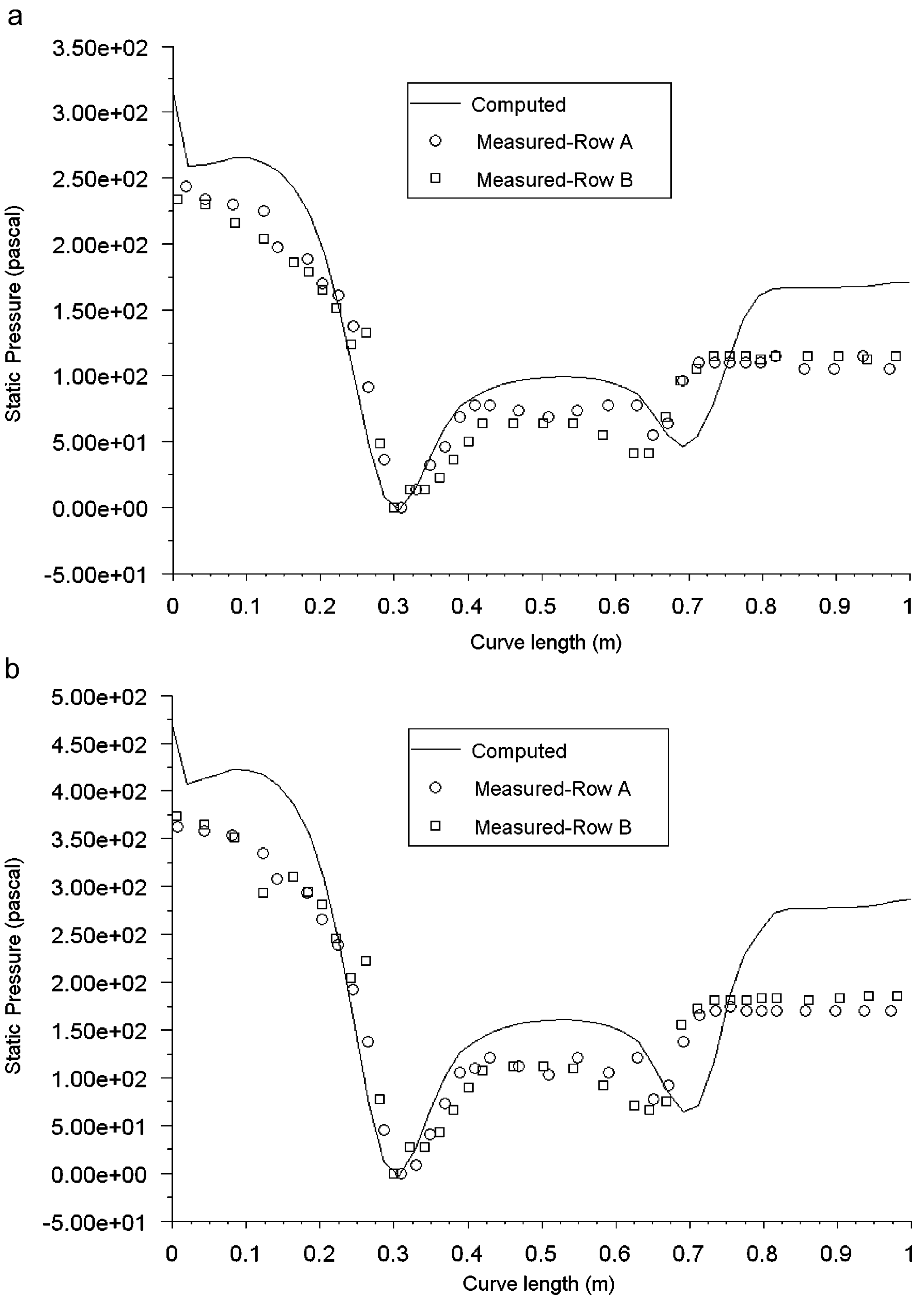

Fig. 7. The pressure distribution along the flow direction inside the scoop at two wind speeds. (a) Airflow speed: 11.25 and (b) airflow speed: $13.9\,\mathrm{m\,s^{-1}}$.

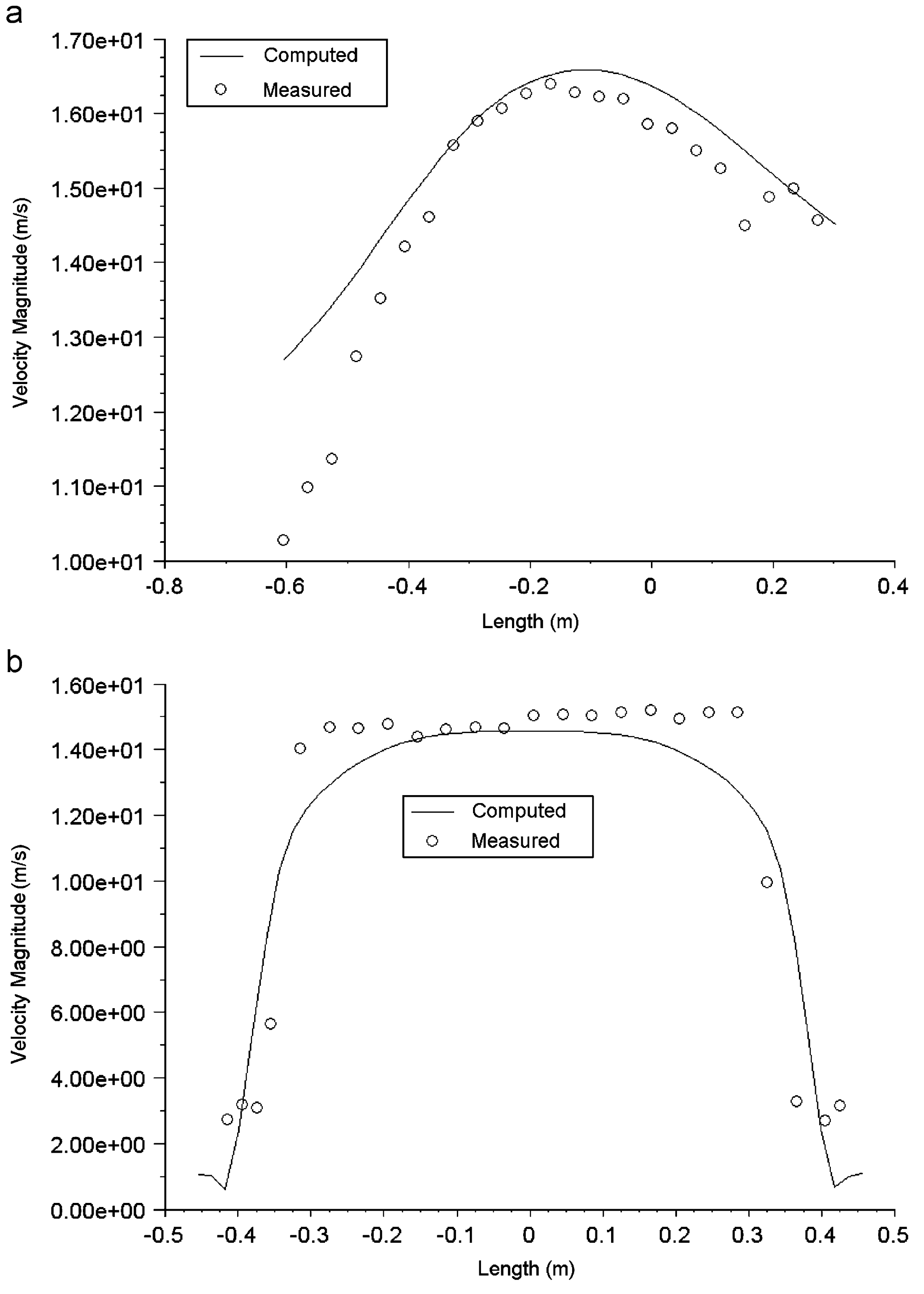

Fig. 8. The velocity distribution along the centrelines in parallel (a) and cross to and (b) the flow inside the scoop at airflow speed of $11.25\,\mathrm{m\,s^{-1}}$. (a) The airflow velocity along the central line parallel to the airflow inside the scoop and (b) airflow velocity along the central line cross the outlet of the scoop.

The discrepancy between the two sets of results could be due to the following reasons:

1. The bar supporter holding the hot wire was vibrating in the airflow.
2. The wind in the wind tunnel was fluctuating.
3. During calibration, the position of hot wire was not the same as that of the pitot tube.
4. The measuring points of the hot wire were not aligned with the centreline since the installation of the bar is on the traversing system.
5. The scoop axis was not aligned with the tunnel axis.
6. Above all, the flow around the scoop was confined by the tunnel, which ideally should be much bigger to minimise the blockage effects. The blockage in the CFD was much smaller as the domain was deliberately made bigger.

Despite the differences between the sets of results, both the computation and laboratory tests displayed similar values for the speed ratio between the maximum speed in the scoop U_c and the free stream velocity U_0 for incident speeds of $U_0 = 7$ and $11.25\,\mathrm{m\,s^{-1}}$:

$$\frac{U_c}{U_0} \approx 1.5. \tag{5}$$

So the available wind power ratio at these two positions is proportional to the square of the speed ratio hence:

$$\frac{P_{s,c}}{P_{s,0}} \approx \left(\frac{U_e}{U_0}\right)^2 \approx 2.25. \tag{6}$$

The available wind energy within the scoop could be 2.25 times that in the wind. If a rotor was assumed with better performance and was inside the scoop, more wind energy could be converted into electrical energy. This effect was measured and modelled in the following tests.

3.2. *Wind tunnel tests*

3.2.1. *The small test wind turbine (trimmed Rutland 913)*

The power curves relating to five different wind speeds are shown for Rutland 913, when its blades were trimmed to fit into the scoop. The wind speed with the lowest power coefficient was $7.3\,\mathrm{m\,s^{-1}}$. C_p reached its maximum at one particular tip speed ratio then it began to fall. There always lies a maximum power coefficient for each wind speed. The highest power coefficient, C_p, obtained from tests on the modified rotor is 0.308, found at a wind speed of $13.9\,\mathrm{m\,s^{-1}}$. At this point the tip speed ratio, λ, is only 2.58. The low tip speed ratio and power coefficient mean that the maximum shaft power measured is only 132 W, less than a third of the shaft power achieved from the original rotor, of which blades were not cut short. Since the original Rutland 913 is designed to work for diameter 0.91 m, it should achieve its best performance at its design point. By cutting the blades to a diameter 0.57 m, not only was the swept wind area decreased, but also the performance and efficiency of the blades were lowered. In addition, the nacelle blockage presented a large percentage of the swept area of the trimmed rotor than that of the original one. All the power curves except one at $7.3\,\mathrm{m\,s^{-1}}$ reached the highest C_p at around tip speed ratio 2.5. At a given tip speed ratio, C_p increased with the increase of wind speed except at speed $7.3\,\mathrm{m\,s^{-1}}$.

3.2.2. Trimmed Rutland 913 in the scoop

The power curves relating to eight different wind speeds are also plotted in Fig. 9b for the trimmed Rutland 913 with the scoop. Here the C_p was calculated using 0.91, in

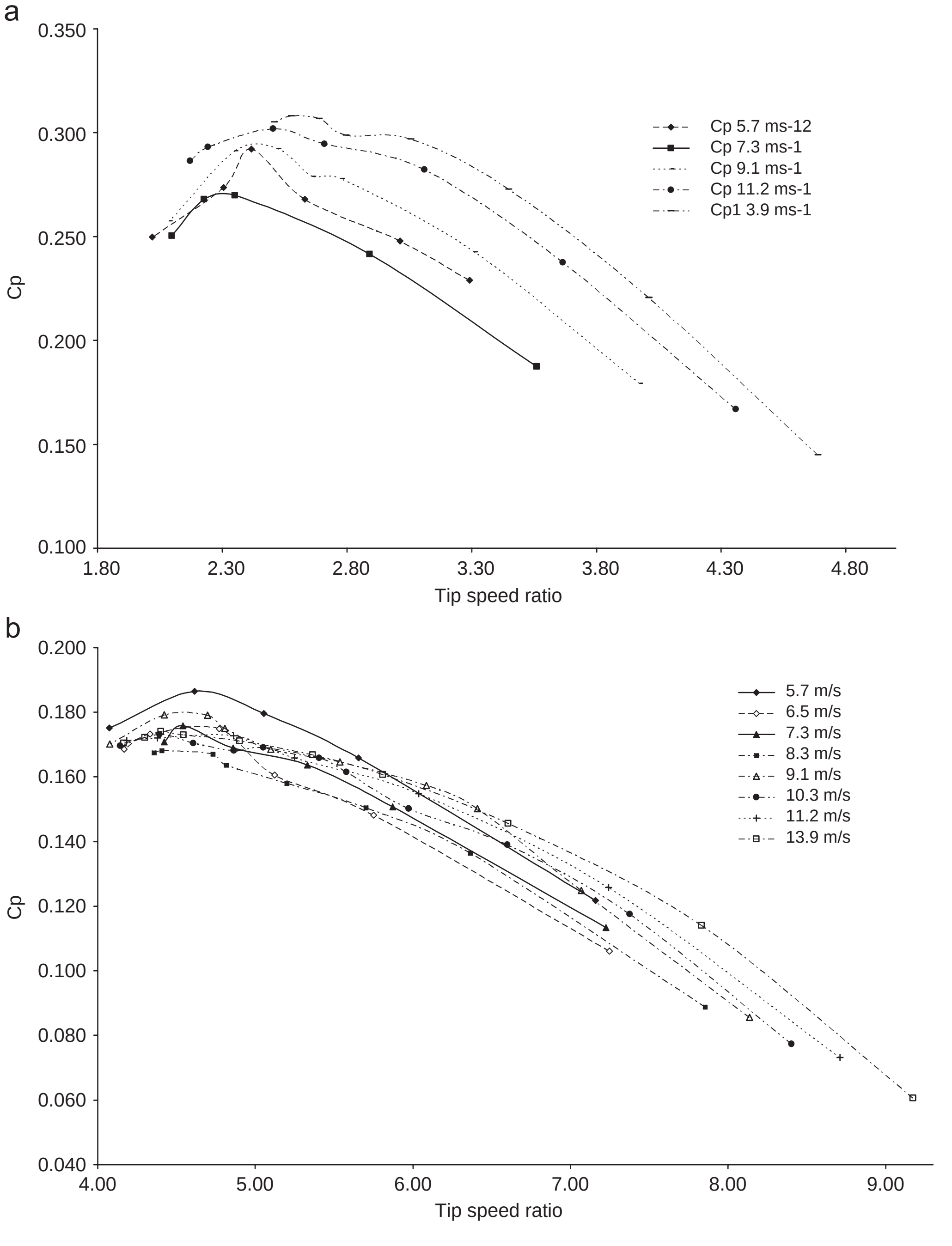

Fig. 9. The power curves for trimmed rotor. (a) With various tip speed ratios and (b) at various test wind speeds.

diameter, the area of scoop to gather the airflow. These curves show that the rotor inside the scoop produced the highest power coefficient, C_p of 0.19 at a free stream speed of $5.7\,m\,s^{-1}$ and tip speed ratio of 4.5. Using a scoop around a rotor had changed the tip speed ratio, which could improve the maximum power coefficient compared with power curves shown in Fig. 9(a). The maximum tip speed ratio was 4.5 compared with 2.5 for the trimmed Rutland 913 alone. Also at a given tip speed ratio, C_p did not increase with wind speed. The highest C_p was achieved at $5.7\,m\,s^{-1}$ which suggests that the rotor and scoop would be more suitable for the low wind speed conditions.

This exercise, plotting C_p against tip ratio, was to find the optimised tip ratio for a particular wind turbine and its configuration. Its additional value is that it suggests that the rotor would need optimising when it is to work inside a scoop to achieve the optimal ratio. This optimisation would involve design of new blades, rotor, hub, nose cone and nacelle, all components that are aerodynamically significant. It is not appropriate to use the C_p alone to compare the performance of turbines in two different configurations. Further study then would include development of the design rotor as well as a proper criterion to assess the improvement in performance. In this study the power output was temporarily used for comparison.

3.2.3. Maximum power

The maximum power of a wind turbine is tuned for a given wind speed by altering the rotational speed of the rotor. Fig. 10 displays the maximum shaft power generated in the two wind tunnel tests for the trimmed Rutland 913 rotor, one with and the other without the scoop. The figure shows clearly that the higher wind speeds produce greater power for both tests and the use of the scoop improves the power output for this trimmed rotor only. A close look shows that such improvement could be as good as 50% increase in slow winds, from cut-in speed up to about $10\,m\,s^{-1}$. In higher winds, such increases were lower at about 25%. This improvement at low speeds could be very meaningful for micro-wind turbines working in built-up areas, where winds are often low speed. The power curve tests also revealed that the performance of the Rutland 913 was reduced after its blades were made short. Even with the scoop, the power outputs were about 12 and 71 W at 5.15 and $9.8\,m\,s^{-1}$, respectively, lower than the rated figures of the original 913 turbine. The scoop, which was expected to gather the same amount of airflow to drive the rotor to produce the higher power failed. As discussed already in Section 3.2.1 this was because the original design which was optimised for the original diameter could not work more effectively when the blades were trimmed short, which can be proved by the large reduction in C_p discussed in Section 3.2.1. Furthermore, as adding the scoop had the swept area and reference speed, the C_p did not seem to provide an informative comparison. Its use here was to provide the optimised tip speed ratio at various incident speeds. While the power output still seems the ultimate criterion for assessing the performance of a wind turbine, which base this variable is compared to needs further investigation. The conclusion dawn here is that the power of a wind turbine in a scoop can be increased to some degree. Furthermore, a wind turbine with well-designed blades, hub and nacelle could achieve better performance than the non-optimised wind turbine in a scoop and further study is needed.

3.3. CFD validation of trimmed Rutland 913 windcharger

The CFD modelling provides detailed information and visual indication of airflows in various critical areas, which helps understand the aerodynamics of the rotor and the scoop.

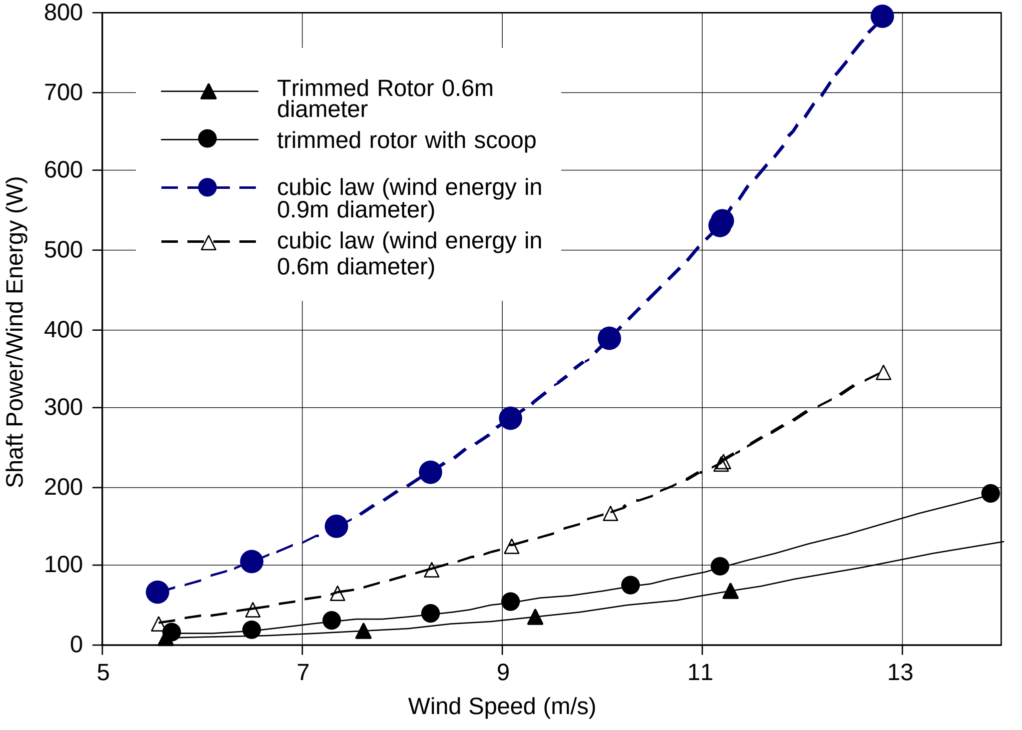

Fig. 10. The maximum shaft power vs. the wind speed for the two tests are plotted with the wind energy cross the same swept areas.

Fig. 11 is a plot of the overall flow field on the central plane of the wind tunnel, characterized by contours and vectors of velocity. The highest velocities are seen at the tip of the rotor in the domain. There was a recirculation zone with lower speeds between the diffuser and contractor due to the restriction caused by the scoop. It can also be seen clearly that the incoming airflow was blocked by the hub cone and the rotor. A circular accelerating zone existed behind the rotor, which resulted in low pressure near the wall of the scoop. Near the rear part of the scoop, there also was a near zero velocity zone which was also identified by the wind tunnel tests. Behind the hub of the rotor, a low-speed region was formed indicating the wake region. Applying the symmetry boundary condition not the periodical boundary conditions on the domain is more suitable since it is clearly seen that the wake region is not periodical. The highest speed in the scoop was found at the interface between the cylindrical section and the diffuser of the scoop, which is clearly revealed by lowest pressure values at the same position in the contours of static pressure, Fig. 12.

Fig. 12 shows the contours of static pressure on the inner wall of the scoop and the pressure decreased along the scoop from the inlet which reveals a lower velocity region in the inlet region and a higher velocity region between the cylinder and diffuser. Fig. 13(a) shows the contours of the total pressure distribution in the wind tunnel which reflects the total energy distribution. The contours of the total pressure show the wake development downstream of the turbine. The wake region is shown behind the wind turbine. The wind

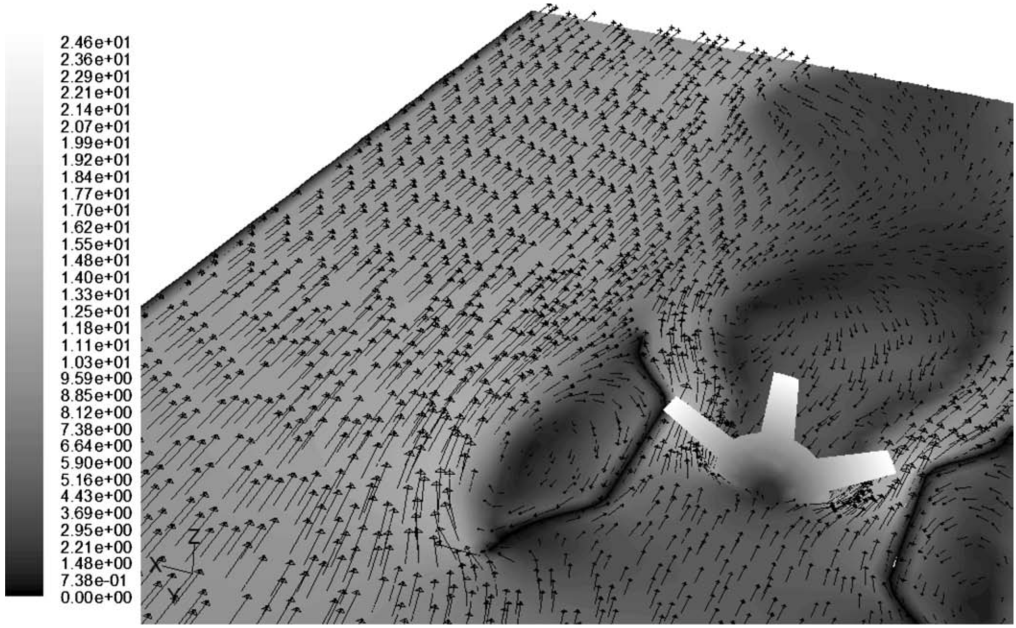

Fig. 11. Contours and vectors of velocity in the scoop.

with high energy entered from the top in the figure and was blocked by the wind turbine which captured most of the wind energy and created a wake region behind the wind turbine. Fig. 13(b) shows the axial velocity distribution on planes passing through closely spaced turbine, revealing the strong wake effect downstream. The axial velocity contours are used to identify the transition from the near wake to the far wake region. In the far wake, diffusion phenomena caused the overall wake cross section to expand while the de-energized core in the central region reduced.

To validate the CFD model, the pressure was measured again in the test of trimmed rotor in the scoop and compared with the variable computed by the CFD model at a wind speed $11.25\,\mathrm{m\,s^{-1}}$ (Fig. 14a). Referring to the pressure distribution without the rotor in Fig. 7, the existence of the rotor in the scoop radically changed the pressure profile in the scoop. The lowest pressure was both measured and computed at the corner of the interface between the cylinder and the diffuser due to the increase of pressure in the front section. This was associated with a decreased wind speed caused by the hub and rotor restriction. Apart from this turning point, other features of the pressure profile were all similar in both the measured and computed results, although the computed ones at the entrance were constantly lower than the measured. But in general the two sets of pressure profiles of both measured and computed show a good agreement except some small discrepancy in the front section. This provides more confidence in the CFD modelling.

Further confidence was gained by the agreement between the measurement and computed values of the power output, which was the ultimate variable to be obtained from a CFD modelling. For this comparison, Eq. (4) was applied in post-processing of the CFD data to compute the power output: the mechanical power generated at the shaft axis as a function of inlet velocity. The comparison between the measured power outputs and the

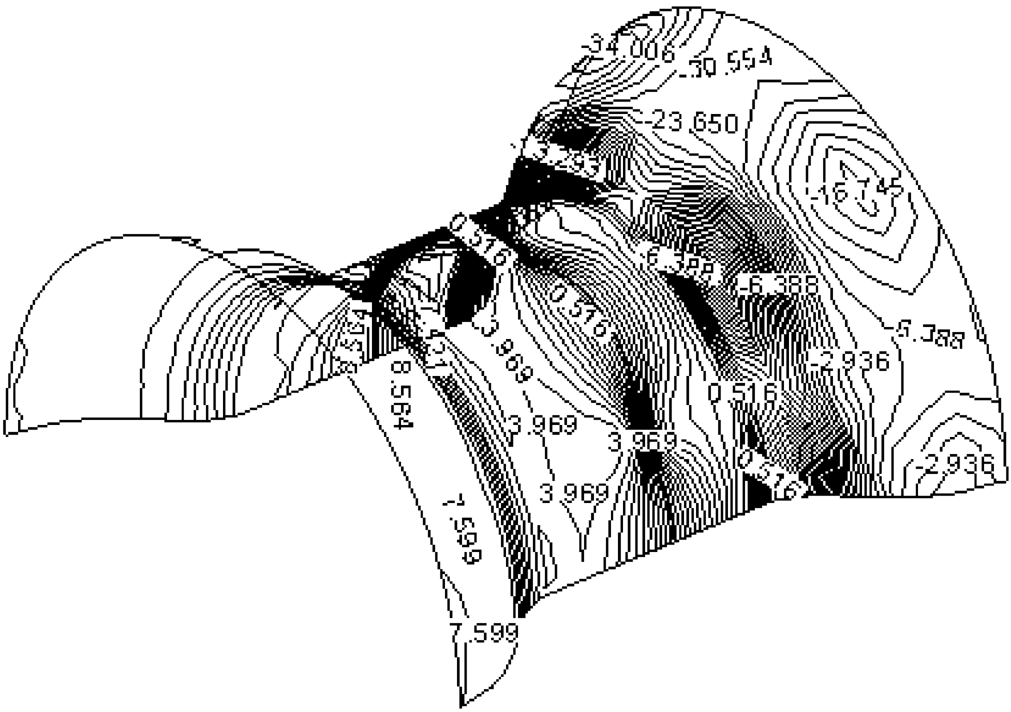

Fig. 12. Contours of static pressure on the scoop.

CFD results were in very good agreement, the errors were within 5%, which suggested the CFD methods developed here would be useful in later computational investigations. The only caution is that the flow domain needs to be large enough to minimise the effects of blockage by the object being tested. This actually is in agreement with the normal rules of thumb of CFD external flow modelling that is applied to minimise the effects of imposing boundary conditions.

In summary, given the rotor geometry and operating characteristics, CFD computation is able to predict the power generated by the rotor in the scoop. Specific modelling, such as finding the optimised blades, nose cones and nacelles, can easily be analyzed using CFD methods. Also three-dimensional simulations of wind turbines can be extended to other situations including landscape topography and different boundary and turbulence profiles.

4. Conclusions

This paper concentrates on the development of the methodology of designing an efficient small domestic wind turbine with a scoop. In this part, both the tests and CFD computations were carried out to validate CFD results. In the tests, the scoop, the trimmed Rutland 913 and the trimmed Rutland 913 operating inside the scoop were used as test cases to validate CFD computations and predict power curves. For the power curve predictions, there lies an optimum tip speed ratio for each incident wind speed in all three rotor tests. The performance of trimmed Rutland 913 windcharger has been dramatically reduced since the swept wind area was reduced. According to these tests, it is proven that

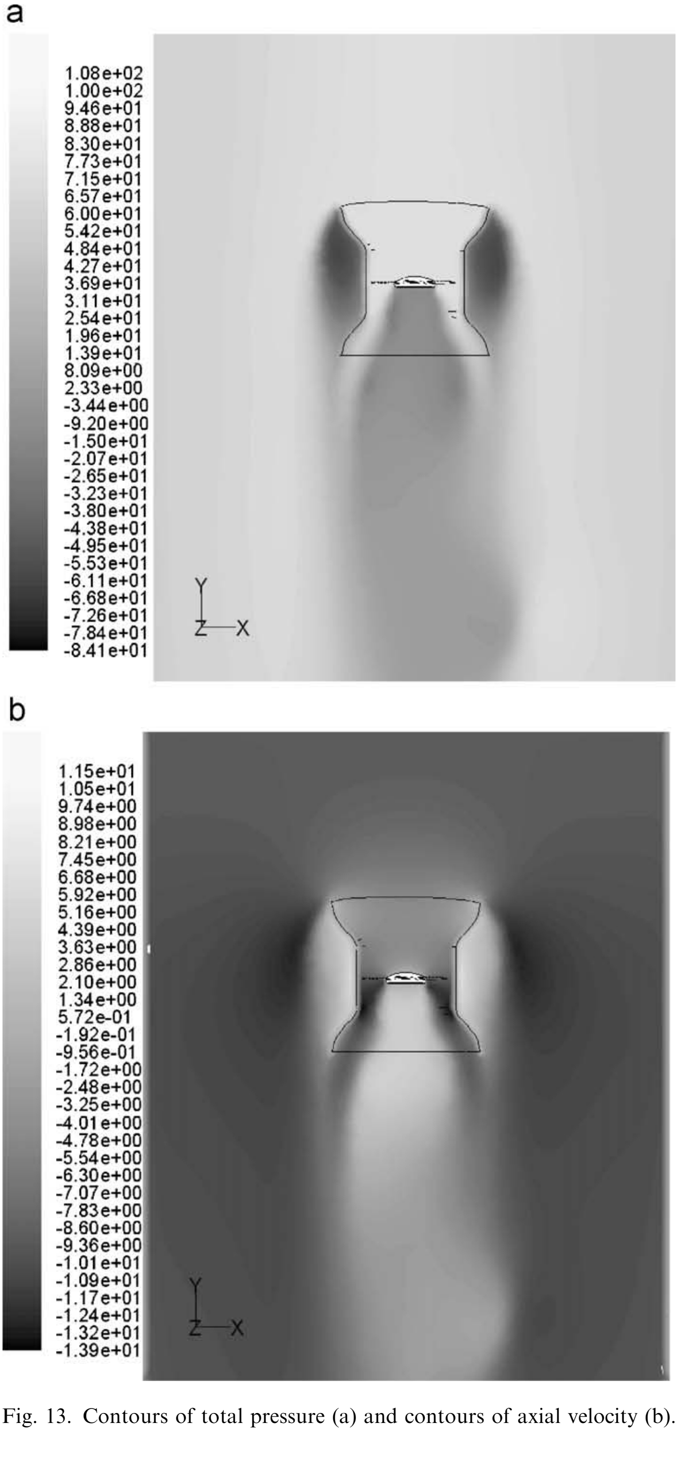

Fig. 13. Contours of total pressure (a) and contours of axial velocity (b).

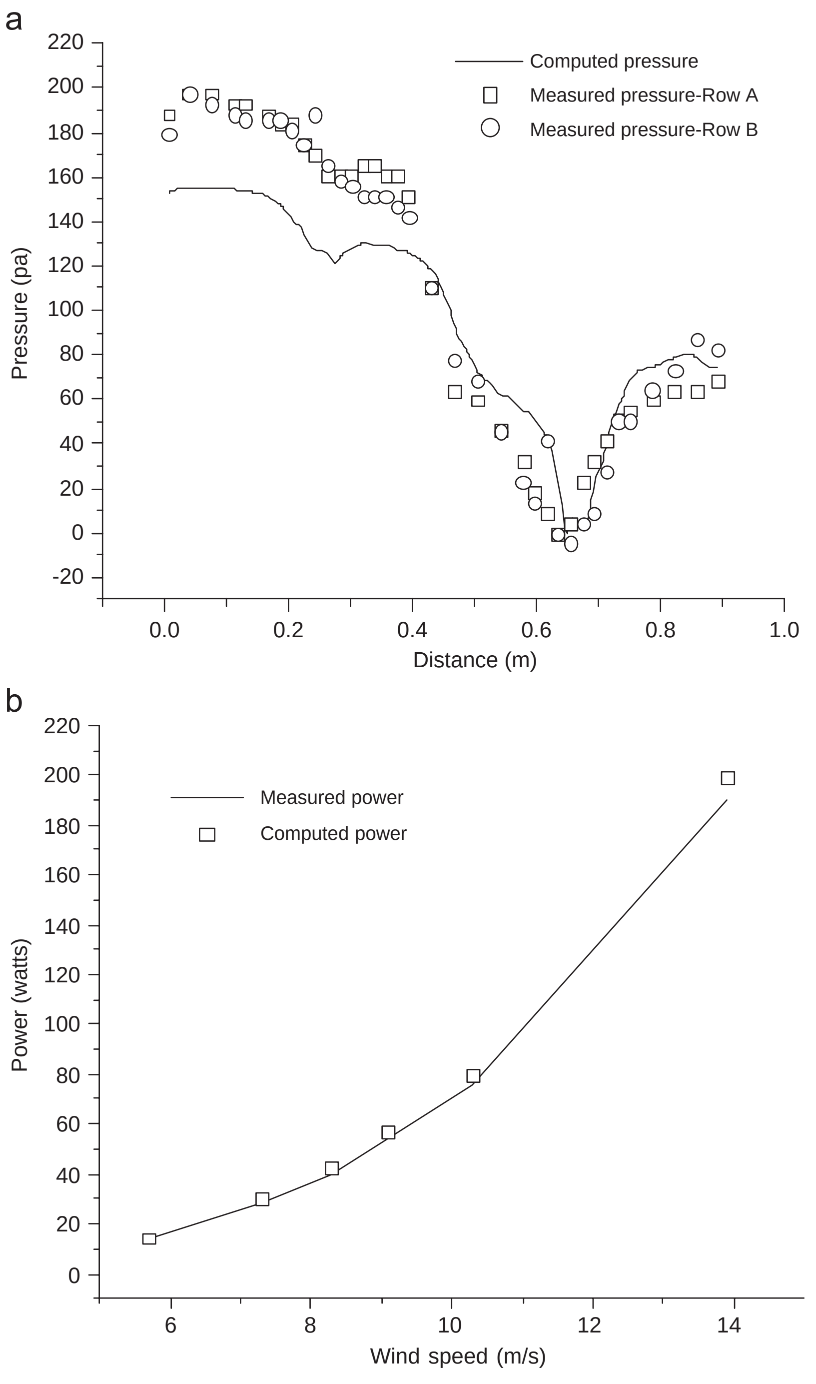

Fig. 14. Comparison between the measured and computed pressure (a) and predicted power output (b). (a) The pressure distribution inside the scoop, (b) the power output vs. wind speed.

the scoop improves the power output of the wind turbine by accelerating the airflow in the cylindrical section. The scoop can perform well, providing a 2.2 times increase in mechanical energy than without a scoop. The CFD computation can provide details of flow and predict the power curves measured in the wind tunnel test. The error between the computation and wind tunnel test is within 5%. CFD methods can be used as an effective design tool for scoop and wind turbine in this methodology.

According to the above investigation, scoop modelling based on CFD was reliable, as the validation confirms accuracy of the computer modelling. Therefore, the findings are acceptable. Scoop 6 is then considered as the optimised scoop for the wind turbine. Out of the scope of this study are other considerations, such as wind load, structural behaviour and cost, which should be taken into account in the development of the actual product.

A wind turbine is always designed to work in certain conditions at which it is most efficient in converting wind energy into electricity. Any alternation could substantially change its performance. This was confirmed in the wind tunnel tests for the Rutland 913. This justifies the need to design specific blade systems, which is only one of the many components that constitute a wind turbine and impact on its performance. Equally important is the design of the generator and control electronics to ensure maximum power production at a given wind speed with adequate response times.

The CFD method can be used as a virtual wind tunnel and this has been validated. It is now being used to test the proposed rotor design options, including hub shapes and blades configuration. This research will be discussed in Part 2.

Acknowledgements

This study was supported by Scottish Executive through its SME Collaborative Research Programme (SCORE). The authors acknowledge the help offered during the period of study by the following people: Jim Laing, Scottish Executive Fife, and Robert Bruce, Strategic Business Development Manager, Technology & Research Services (TRS), Heriot-Watt University.

References

Abe, K., Nishida, M., Sakurai, A., Ohya, Y., Kihara, H., Wada, E., Sato, K., 2004. Experimental and numerical investigations of flow fields behind a small wind turbine with a flanged diffuser. J. Wind Eng. Ind. Aerodyn. 92, 315–330.

Abe, K., Nishidab, M., Sakuraia, A., Ohyac, Y., Kiharaa, H., Wadad, E., Satod, K., 2005. Experimental and numerical investigations of flow fields behind a small wind turbine with a flanged diffuser. J. Wind Eng. Ind. Aerodyn. 93, 951–970.

Ackermann, T., Soder, L., 2002. An overview of wind energy-Status 2002. Renew. Sustain Energy Rev. 6, 67–128.

American Wind Energy Association (AWEA), 2002. The US Small Wind Turbine Industry, Roadmap, A 20-Year Industry Plan for Small Wind Turbine Technology. American Wind Energy Association (AWEA).

Beattie, A., 2001. Wind turbine power performance assessment under real conditions. Dissertation. Loughborouth University.

Clausen, P.H., Wood, D.H., 2000. Recent advances in small wind turbine technology. Wind Eng. 24 (3), 189–201.

Corbus, D., Link, H., Butterfield, S., Stork, C., Newcomb, C., Sasseen, T., 1999. Certification testing for small wind turbines. In: Proceedings of Windpower '99 Burlington, Vermont, June 20–23, 1999.

Ebert, P.R., Wood, D.H., 1997. Observations of the starting behaviour of a small horizontal-axis wind turbine. Renew. Energy 12 (3), 245–257.

European Commission, 2004. Catalogue of European Urban Wind Turbine Manufacturers, the European Commission under the Intelligent Energy—Europe Programme.

Fabiano, D.A., Gustavo de Marsillac, P., Villar Alé, G.A., Simioni, G.S., 2003. Power Curve of Small Wind Turbine Generators—Laboratory and Field Testing. World Climate & Energy Event, 1–5 December 2003, Rio de Janeiro, Brazil.

Frandsen, P., et al., 2000. Redefinition power curve for more accurate performance assessment of wind farms. Wind Energy 3, 81–111.

Gilbert, B.L., Foreman, K.M., 1983. Experiments with a diffuser-augmented model wind turbine. Trans. ASME J. Energy Res. Technol. 105, 46–53.

Hansen, M.O.L., Sorensen, N.N., Flay, R.G.J., 2000. Effect of placing a diffuser around a wind turbine. Wind Energy 3, 207–213.

IEC Standard 61400-2, 1996. International Electrotechnical Commission (IEC), Wind Turbine Generator Systems Part 2: Wind Turbine.

IEC Standard 61400-12, 1997. International Electrotechnical Commission (IEC), Wind Turbine Generator Systems Part 12—Wind Turbines Power Performance Testing: Wind Turbine, 88/66/CDV.

Imamura, H., Matsumiya, H., Yamada, S., 1999. Method of performance evaluation of a WTGS in Complex Terrain. In: Proceedings of the third Joints Fluids Engineering Conference July 1999, San Fransisco.

Kume, H., Ohya, Y., Karasudani, T., Watanabe, K., 2003. Design of a shrouded wind turbine with brimmed diffuser using CFD. In: Proceedings of the Annual Conference of JSAS, The West Side Division. pp. 51–54.

Mandas, N., Carcangiu, C.E., Cambuli, F., 2005. Department of Mechanical Engineering, Università degli Studi di Cagliari, Cagliari, Fluent NEWS, Summer 2005.

Matsushima, T., Takagi, S., Muroyama, S., 2006. Characteristics of a highly efficient propeller type small wind turbine with a diffuser. Renew. Energy 31 (9), 1343–1354.

Mayer, C., Bechly, M.E., Hampsey, M., Wood, D.H., 2001. The starting behaviour of a small horizontal-axis wind turbine. Renew. Energy 22, 411–417.

Ohya, Y., Karasudani, T., Sakurai, A., 2002. Development of high-performance wind turbine with brimmed diffuser. J. Jpn. Soc. Aeronaut. Space Sci. 50, 477–482 (in Japanese).

Ohya, Y., Karasudani, T., Sakurai, A., Inoue, M., 2004. Development of high-performance wind turbine with a brimmed-diffuser: Part 2. J. Jpn. Soc. Aeronaut. Space Sci. 52, 210–213 (in Japanese).

Phillips, D.G., Richards, P.J., Flay, R.G.J., 2000. CFD modelling and the development of the diffuser augmented wind turbine. In: Proceedings of the Computational Wind Engineering, 2000, Birmingham, pp. 189–192.

PROVEN, 2006. WT600, Product Specifications, ⟨http://www.provenenergy.co.uk⟩

Riso, 2001. European Wind Turbine Testing Procedure Developments—Task 1: Measurement Method to Verify Wind Turbine Performance Characteristics, Riso-R-1209(EN).

Sorensen, J.N., Kock, C.W., 2004. A model for unsteady rotor aerodynamics using CFD. J. Wind Eng. Ind. Aerodyn. 92, 315–330.

Swift Wind, 2006. Product Specifications, ⟨http://www.renewabledevices.com/⟩

Wood, D.H., 2001. A blade element estimation of the cut-in wind speed of a small turbine. Wind Energy 25 (4), 249–255.

Wright, A.K., Wood, D.H., 2004. The starting and low wind speed behaviour of a small horizontal axis wind turbine. J. Wind Eng. Ind. Aerodyn. 92, 1265–1279.